APPLIED SCIENCES AND ENGINEERING

Visualization of vermilion degradation using pump-probe microscopy

Jin Yu[1], Warren S. Warren[1,2,3,4], Martin C. Fischer[1,4]*

Here, we demonstrate the use of pump-probe microscopy for high-resolution studies of vermilion degradation. Vermilion (mostly α-HgS), an important red pigment used in historical paintings, blackens over time, and metallic Hg and β-HgS have been implicated as possible degradation products. Conventional analysis techniques have trouble differentiating α- and β-HgS with sufficiently high spatial resolution. However, pump-probe microscopy can differentiate metallic mercury, α- and β-HgS, and map each distribution on the microscopic scale. We studied artificial degradation of α-HgS; femtosecond-pulsed laser irradiation induces an irreversible phase shift of α- to β-HgS, in which the initial presence of β-HgS grains can increase the rate of conversion in their vicinity. Continuous ultraviolet exposure instead generates both liquid Hg and β-HgS, with a conversion rate that increases with elevated temperatures. Last, we reveal the presence of β-HgS as a natural degradation product in discolored vermilion layers in a 14th century Italian painting.

INTRODUCTION

Mercury sulfide, HgS, has two major solid-phase forms, each having a distinctive color: α-HgS (cinnabar, trigonal) is red, while β-HgS (metacinnabar, cubic) is black (see Supplementary Materials for reflectance spectra) (*1*–*6*). Vermilion (mostly the ground form α-HgS) has been globally used as a pigment in historical paintings due to its vivid red color, but under natural lighting and illumination conditions, it can experience darkening over time (*7*–*9*). This darkening, which can alter an artwork's appearance from the artist's intent, has prompted studies of the underlying degradation process. Metallic mercury (Hg) (*10*–*12*) and β-HgS (*10*, *13*–*15*) have been considered as possible degradation products of vermilion, leading to the loss of the red color. Early experiments on pulsed laser ablation have observed a phase change of α- to β-HgS under intense light exposure (*16*, *17*), resulting in the appearance of black regions. In the absence of light, such an irreversible phase conversion can be induced in vermilion samples heated to temperatures more than 350°C (*1*, *3*, *4*, *18*, *19*), raising the question of how such a process might arise under natural light exposure at room temperature. More recently, x-ray and electrochemical studies have revealed that chloride can act as a catalyzer (*10*–*12*, *20*, *21*) for the light-induced breakdown of α-HgS to metallic Hg, also leading to a loss of vermilion's red color (*7*, *11*, *12*, *22*). Microscopic studies of samples from historical paintings have shown the presence of high chloride concentration in the vicinity of some degraded areas (*23*, *24*), but the origin of the chloride is speculative. In microscopic studies, elemental analysis techniques (e.g., x-ray fluorescence) (*25*) and scanning electron microscopy with energy-dispersive x-ray spectroscopy (SEM-EDS) (*10*, *23*) can detect changes in elemental ratios in degradation products (e.g.,, α-HgS versus Hg), but the identical elemental composition of α- and β-HgS prevents differentiation. Other x-ray analysis techniques, such as x-ray diffraction (XRD) (*17*, *18*, *26*, *27*) and x-ray photoelectron spectroscopy (*16*, *28*), can differentiate the two phases, but obtaining layer-level or even grain-level spatial resolution is challenging and requires complex instrumentation [synchrotron (*12*, *25*, *29*)]. Here, we demonstrate the use of femtosecond (fs) pump-probe optical microscopy as a new tool to study the degradation mechanisms of vermilion in paint layers with micrometer voxel sampling.

The principle of optical pump-probe microscopy is detailed in a recent review (*30*) and will be described only briefly here (for more details, see fig. S1). An intensity-modulated pulse train of fs pulses (pump) and a synchronized fs pulse train of different wavelength (probe) are spatially superimposed and interact with the sample in the focal region of the microscope. Nonlinear optical interactions between the light and sample (vermilion) transfer some of the pump modulation to the probe. To measure the interaction, we recorded the modulation on the back-scattered probe light as a function of the pump-probe interpulse time delay (τ). Nonlinear interactions that can be measured with this pump-probe technique include effects that occur during pulse overlap, such as two-photon absorption (TPA; absorption of a pump and a probe photon) and stimulated Raman scattering. Pump-probe (sometimes termed transient absorption) can also measure interactions that involve population dynamics at delays longer than the pulse duration, such as excited-state absorption (ESA), ground-state depletion (GSD; the competition between two transitions from the ground state), and stimulated emission. The combination of accessible electronic and vibrational processes offers the promise of spectral and temporal signatures that can be molecular specific at high spatial resolution in three dimensions. We have previously described this technique's ability to create virtual depth sections in paint samples and paintings (*31*–*33*). However, all data here were acquired within about 10 μm of the sample surface.

RESULTS AND DISCUSSION

Pump-probe signatures of α-HgS, β-HgS, and metallic Hg

To obtain reference pump-probe signals, we acquired a series of pump-probe images of ground red HgS powder, ground black HgS powder, and liquid Hg suspended between two glass surfaces (Fig. 1, A to C). We observed that all samples have distinctive nonlinear signatures at the pump-probe wavelengths of 720 and 817 nm (Fig. 1D). Red HgS primarily exhibits TPA during temporal pulse

[1]Department of Chemistry, Duke University, Durham, NC 27708, USA. [2]Departments of Radiology, Duke University, Durham, NC 27710, USA. [3]Department of Biomedical Engineering, Duke University, Durham, NC 27708, USA. [4]Department of Physics, Duke University, Durham, NC 27708, USA.
*Corresponding author. Email: martin.fischer@duke.edu

overlap—one-photon transitions at these wavelengths do not occur since the energies are outside the absorption band (see fig. S2 for linear reflectance spectra of red and black HgS). In addition, note that pump-probe only measures TPA that removes at least one photon from each (pump and probe) beam. Black HgS and liquid Hg produce a strong negative signal that persists for longer delay times (GSD); liquid Hg produces additional positive ESA signals for even longer delays. While pump-probe images of black HgS and liquid Hg show fairly uniform pump-probe responses in the entire field of view (FOV), the microscopic image in Fig. 1A shows that the red HgS powder contains small amounts of material that exhibit pump-probe signatures identical to black HgS (the delay curve is also included in Fig. 1D). We conclude that the black HgS is uniformly β-HgS and attribute the minor component in the red HgS (predominantly α-HgS) to the presence of a few β-HgS grains. When switching the pump and probe wavelengths (817-nm pump/720-nm probe; fig. S2), the negative signal from β-HgS persists, pointing to GSD as the signal origin (for such a switch, stimulated emission would be suppressed, while stimulated Raman scattering signals would change sign). Figure 1 highlights the advantage of microscopic analysis over transient absorption spectroscopy, which inherently has much lower spatial resolution (typically tens of micrometers or larger)—the small contributions of β-HgS are not observable in a spectrum averaged over a large region.

Laser-induced phase conversion

As known from laser ablation experiments (*16*, *17*), intense laser pulses can induce the conversion from α- to β-HgS. To confirm this effect under fs illumination and to determine damage threshold values for our imaging studies, we deliberately increased our laser illumination powers (see experimental details in the Supplementary Materials). Figure 2 (A to C) shows a series of images acquired before and after laser-induced degradation above the damage threshold of 0.45 mW in each beam (see Materials and Methods for power conversions). In the reference image before degradation (Fig. 2A), we observe a few grains of β-HgS. After high-power illumination, we see the conversion of positive TPA signal of α-HgS to negative GSD signals of β-HgS (Fig. 2, B and C). The areas of conversion seem to emanate from areas that already contain grains of β-HgS, which act as seeds for conversion. After laser-induced degradation, we confirmed that the illuminated areas of the sample visually appear black and that the GSD signals in the degraded areas are similar to those of black HgS (see details in fig. S3).

To further validate the observed conversion from α- to β-HgS under strong fs-laser pulse exposure, we performed XRD and SEM-EDS analysis on red HgS, black HgS, and red HgS that turned dark during laser-induced degradation. Because our XRD instrument does not offer microscopic resolution, we degraded a large area (size, 2 cm by 2 cm; see the image in fig. S3) for analysis. The diffraction pattern of red and black HgS correspond to reported patterns of α- and β-HgS, respectively (*17*, *18*, *26*). Figure 2D shows the region around 31°, which shows the most marked difference (see fig. S3 for the full spectrum). The spectrum of red HgS after laser degradation is also plotted and shows components of β-HgS. Note that the induced degradation is only partial (only on the surface), while XRD probes the entire sample volume. Figure 2E shows EDS spectra of the three samples, where the ratio between Hg and S can be identified with peaks of Hg (M_α, 2.195 eV and M_β, 2.281 eV) and S (K_α, 2.309 eV and K_β, 2.465 eV). Insignificant changes on Cl peak intensities at 2.622 eV (K_α) provide insufficient information about the Cl-assisted phase conversion. The EDS analysis indicates that fs-laser–induced degradation preserves the Hg/S ratio of intact red and black HgS.

In some regions that underwent a transition from instantaneous (positive) TPA to long-lived (negative) GSD signal, we observed a long-lived, positive ESA signal right before the signal turned into negative GSD (Fig. 2F; see more details in fig. S5). We can observe not only the initial strong TPA signal but also the ESA signal that persists for longer delays. After acquiring a number of images at increasing delay times, the ESA signal disappears and turns into GSD (this happened to an image corresponding to various time delays); after that time, the signal stayed negative. We attribute this temporary positive noninstantaneous ESA signal to an intermediate state (chemical or phase) occurring during the phase transition from α- to β-HgS. Samples with induced long-lived ESA signals were repeatedly imaged (at low-power levels to prevent further conversion). We have not observed appreciable changes over the time scale of 5 weeks

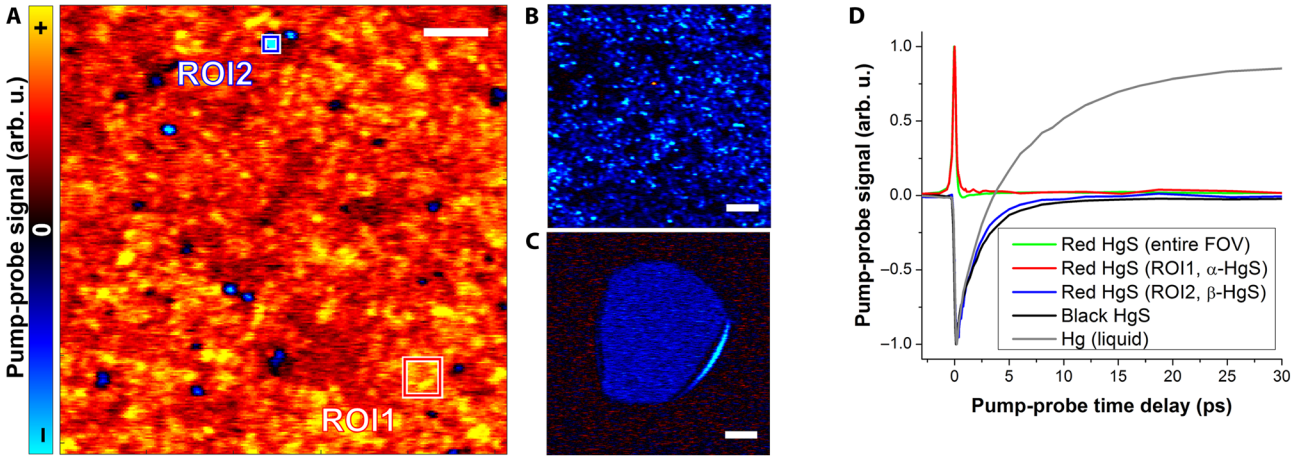

Fig. 1. Pump-probe signatures of vermilion (red HgS), black HgS, and metallic Hg. Pump-probe images acquired at a pump-probe wavelength of 720 and 817 nm of (**A**) red HgS, (**B**) black HgS, and (**C**) metallic mercury. Interpulse delay τ is 0 (A), 220 (B), and 200 fs (C), respectively. Scale bars, 10 μm. (**D**) Pump-probe (transient absorption) signals as a function of interpulse delays averaged over the entire FOV in (A) to (C). An example of ROI in red HgS [marked in (A)] that exhibits the signals of black HgS is also shown. Arb. u., arbitrary unit.

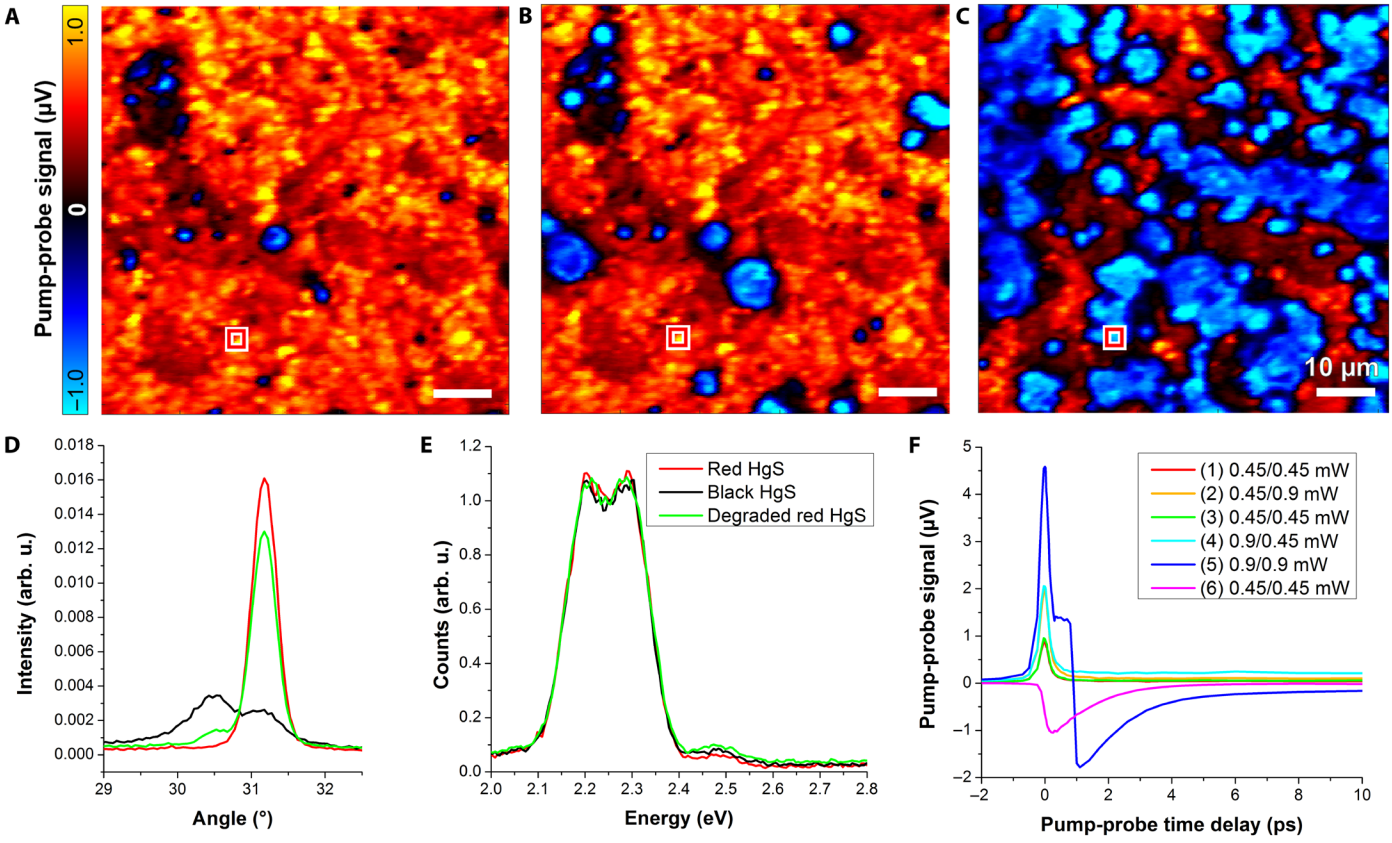

Fig. 2. Characterization of fs-laser–induced degradation. (**A** to **C**) The change on the surface of red HgS powder after excessive exposure to fs-laser power. All images were taken under identical conditions (720 and 817 nm, 0.45/0.45 mW, $\tau = 60$ fs). (A) The initial status of red HgS. (B) The surface changes after inducing degradation at powers of 0.45/0.90 mW. (C) After inducing further degradation at powers of 0.45/0.9 and 0.9/0.9 mW. (**D**) XRD spectra of red, black, and degraded red HgS powder for angles near 30.5°. (**E**) EDS spectra of the same samples (signals were normalized by photon counts at 2.309 eV; see fig. S4 for the corresponding SEM images). All samples show similar Hg and S peak intensities at 2.195 (Hg, M_α), 2.281 (Hg, M_β), 2.309 (S, K_α), and 2.465 eV (S, K_β) and show a negligible amount of Cl peak intensities at 2.622 eV (Cl, K_α). (**F**) Occurrence of a positive ESA signal in regions that turn from α- to β-HgS. Signals were extracted from the fixed ROI [marked in (A) to (C)] of a series of images acquired at different power levels (the number in parenthesis indicates the order of acquisition, followed by the power levels).

(fig. S5), thus placing an approximate lower bound on the lifetime of the intermediate state.

α-HgS in red HgS exhibits only TPA at our pump-probe wavelength combination, while black HgS shows linear absorption at both. To investigate the role of linear and nonlinear absorption during fs-laser–induced degradation, we conducted two imaging studies with different pulse durations and dwell times. In a first comparison, we induced degradation in red HgS with laser pulse of durations 150 and 1 ps with identical average power. The shorter pulses caused appreciable α- to β-HgS conversion, while for longer pulses, the changes were insignificant (fig. S6). In both cases, the total deposited energy is the same, yet the nonlinear interaction is stronger for shorter pulses (the peak intensity scales with the inverse of the pulse duration). Hence, nonlinear absorption (most likely TPA) appears to be the major contributor to fs-laser–induced degradation. In another experiment, we doubled the illumination power (from 0.5/0.5 to 1/1 mW) while reducing the pixel dwell time to half (from 20 to 10 μs), keeping the total linear exposure the same. The high-power case caused more conversion, again implicating nonlinear absorption as the likely cause. During these degradation studies, we observed that the conversion from α- to β-HgS seems to be seeded by the presence of β-HgS grains (see also Fig. 2). A possible explanation is that higher temperatures enhance the rate of light-induced conversion. Since we could not heat and image the sample at the same time in our microscope, we could not verify this hypothesis. β-HgS exhibits linear absorption, hereby creating local heating upon exposure. This, in turn, raises the temperature in the vicinity, which, in turn, would increase the conversion rate of nearby α-HgS. The observation of sputtered black grains on the coverslip of the sample after exposure hints at a substantial temperature increase, but we were not equipped to quantify the temperature during the short laser exposure. From our experiments, the conversion does not seem to be caused by heating due to linear or nonlinear absorption alone (the conversion is initiated via a nonlinear optical process, yet the two-photon cross section is too small for an appreciable temperature increase) but likely involves a multiphoton-induced, temperature-sensitive photochemical reaction. We are planning further experiments to characterize this conversion, including the dependence of the conversion rate on the grain size (which in our current studies was not controlled).

UV-induced degradation

While degradation during fs-laser exposure needs to be understood for pump-probe imaging studies, it is of little concern under normal environmental conditions. To demonstrate that continuous wave

ultraviolet (UV) light (which might be encountered in natural lighting) can induce similar vermilion darkening, we exposed red HgS powder to artificial lighting.

In a first setup, we placed red HgS on a microscope slide and exposed it with a UV light delivered through a fiber bundle (for details, see Supplementary Materials). After exposure, the slide was transferred to the microscope for imaging. The region that received a low dose of UV light showed the appearance of a long-lived ESA signal, in addition to the instantaneous TPA signal (Fig. 3, A and B), similar to the behavior that we observed for fs-induced degradation. Regions that received a larger dose of UV light underwent a complete transformation from TPA to the long-lived negative GSD signal of β-HgS. To confirm this gradual signal change, we performed an experiment where we delivered a smaller amount of UV light through the optical system in the microscope onto a mounted powder sample and intermittently performed pump-probe imaging. Again, we observed the gradual formation of the long-lived positive ESA signal (Fig. 3C). Because of limitations in the microscope optics, we could not deliver enough UV light to cause complete phase conversion. Regions that showed ESA signals seem to be more susceptible to phase conversion to β-HgS for increased fs-laser exposure (fig. S7).

To study the effect of increased UV exposure and the effect of temperature, we placed red HgS powder in a vial, placed the vial on a temperature-controlled hot plate, and illuminated the powder with UV light at higher power levels (for details, see Materials and Methods and fig. S8A). After exposure, the visibly darkened powder was transferred onto a slide for pump-probe imaging. Figure 3D shows a pump-probe image of UV-degraded red HgS, showing large areas of signals that identify β-HgS. Figure 3E shows pump-probe delay curves averaged over the entire FOV, indicating a decrease of positive instantaneous TPA signal (α-HgS) and an increase of long-lived negative GSD signal (β-HgS). This effect is more pronounced for UV exposure at elevated temperatures. In contrast to pump-probe imaging, XRD spectra provided little information about the phase conversion, except for a slight peak broadening near 30.5° (Fig. 3F). During the UV exposure in the vial, a haze of silver droplets had developed along with powder debris. SEM-EDS on the bulk powder detected a decrease of sulfur fraction, while it identified the haze as liquid Hg droplets. Using pump-probe imaging on the haze deposits, we identified liquid Hg droplets and β-HgS debris (see details in fig. S8). Note that in the powder, we did not detect clear pump-probe signatures of liquid Hg.

Pump-probe study in areas of discolored vermilion layers in a 14th century painting

Last, we conducted pump-probe spectroscopic/microscopic analyses on a cross-section from a 14th century painting [*St. John the Evangelist Reproving the Philosopher Crato* by Francescuccio di Cecco

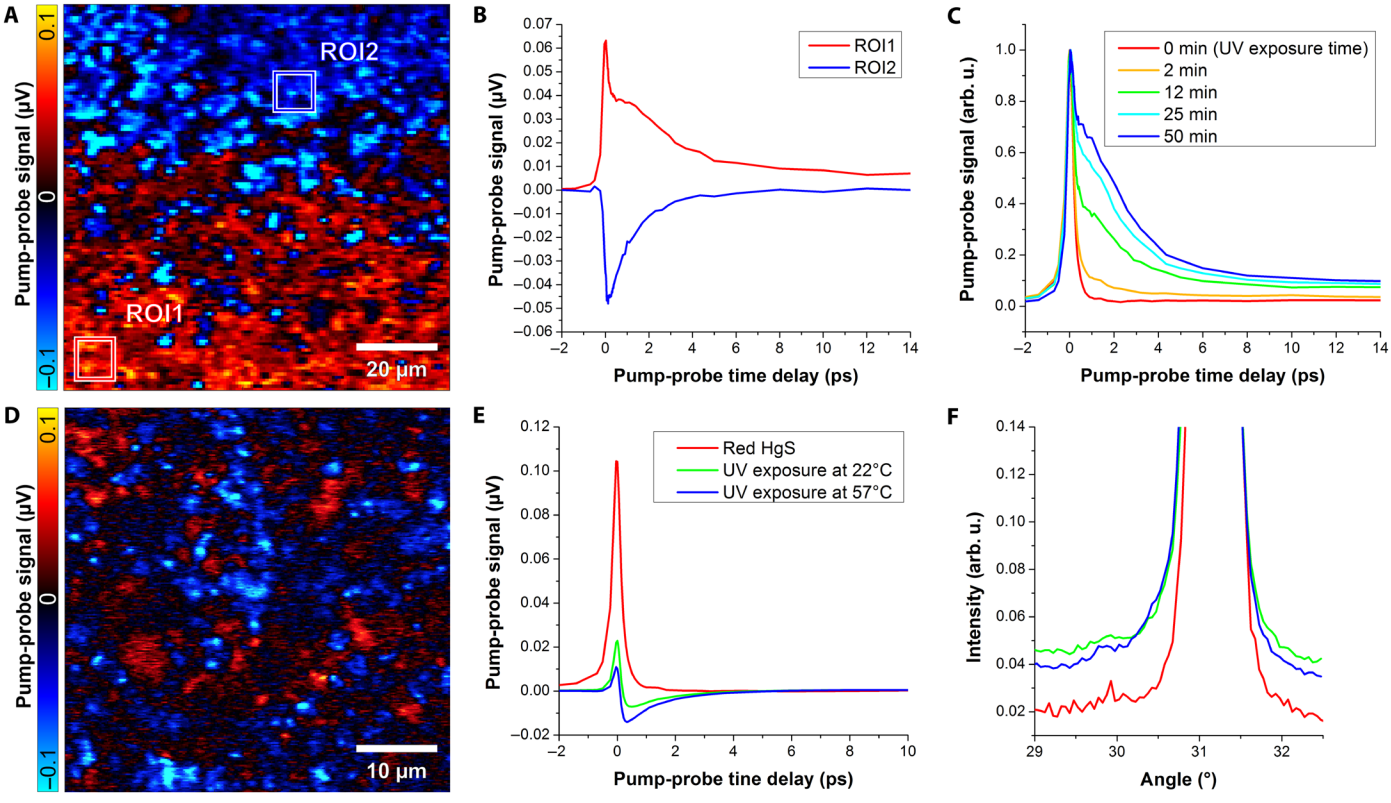

Fig. 3. UV-induced vermilion degradation. (**A**) Pump-probe imaging of UV-exposed red HgS powder on a glass slide. The upper part (ROI2) received more UV light than the lower part (ROI1). After UV exposure, the sample was transferred to the microscope for imaging (720 and 817 nm, 0.2 mW/0.2 mW, $\tau = 140$ fs). (**B**) Pump-probe signals of marked regions in (A). (**C**) Pump-probe signals during UV-exposure of red HgS powder on a slide during imaging. Signals were monitored using 720 and 817 nm, 0.3 mW each. (**D**) A pump-probe image of red HgS powder that was UV-exposed in a vial at 57°C showing a large fraction of negative GSD (720 and 817 nm, 0.3 mW each, $\tau = 120$ fs). (**E**) Pump-probe spectra of undegraded and UV-degraded red HgS (UV exposure in a vial at two temperatures: 22° and 57°C; see more details in fig. S9). (**F**) XRD spectra of the degraded sample showed a broadening of the XRD peak near 30.5° but provided insufficient information about the phase conversion. Signals normalized to the peak at 31.2°.

Ghissi (1375), egg tempera on panel, North Carolina Museum of Art (cross-section size, 1 mm by 0.3 mm); Fig. 4A], which contains areas that were identified by the conservator as discolored vermilion. The cross-section shows the varnish, vermilion, and ground layers (see insets of Fig. 4B). Pump-probe at 720 and 817 nm only images the vermilion layers, where we can observe areas of increased GSD signals in an area of the visibly discolored vermilion, indicating the presence of β-HgS [region of interest 1 (ROI1) in Fig. 4, B and C]. Moreover, gradual signal variations are observed from the top to deeper vermilion layers, even when no discoloration is visible. The deeper layer has a pump-probe response closely resembling intact α-HgS powder (there is a small additional long-lived ESA signal, which could point to a slight degradation). However, the layers closer to the surface show an increase in ESA signals for delay times in the picosecond range (ROI2 to ROI5; Fig. 4C), similar to the signals we observed during UV illumination of red HgS powder samples in Fig. 3. This signature could indicate incipient degradation of these vermilion layers, especially pronounced toward the surface.

SEM-EDS analysis (see fig. S10) did not reveal noticeable amounts of chloride in any area of the cross section. In areas where we observed

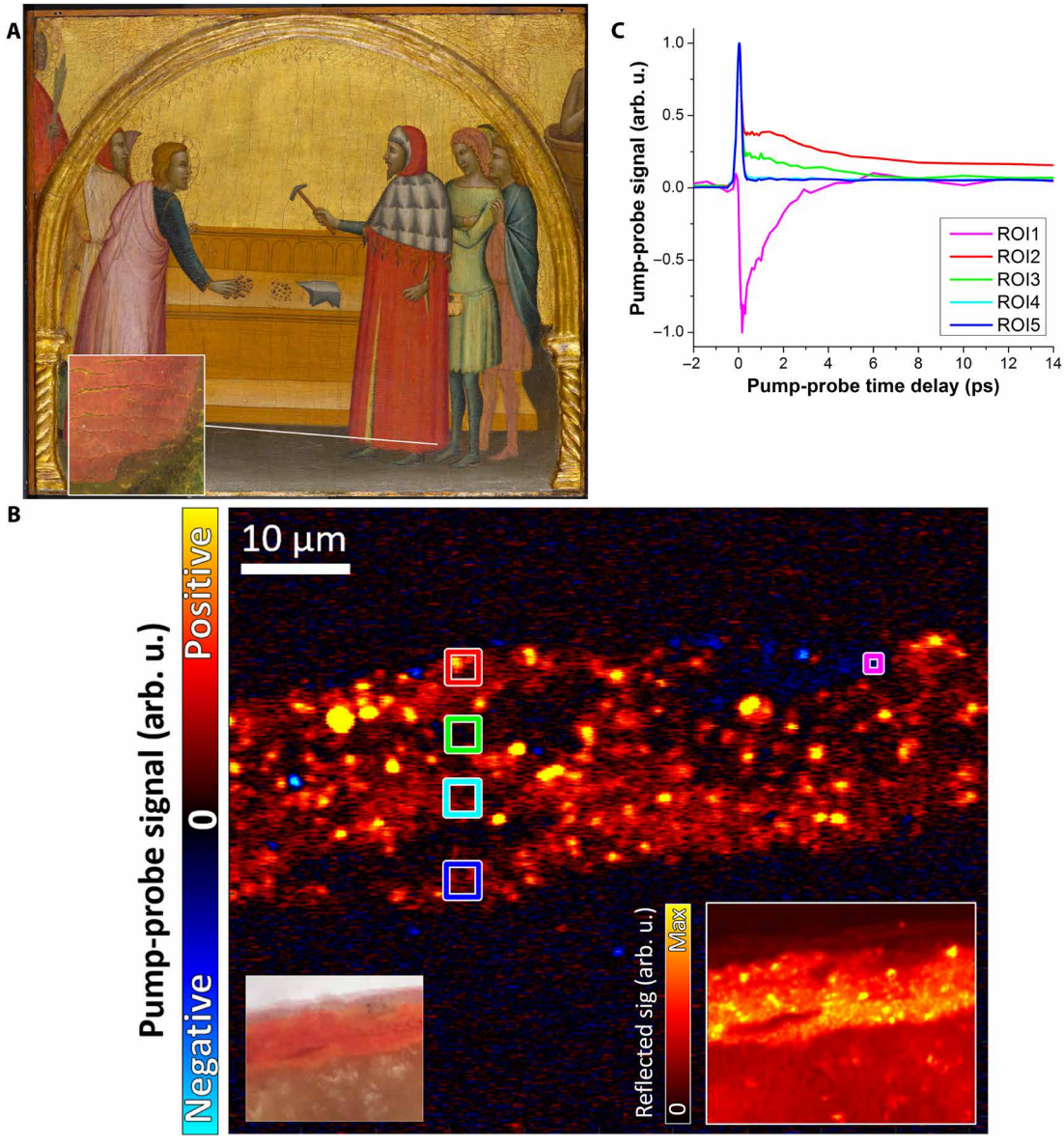

Fig. 4. Degradation products in a 14th century painting containing discolored vermilion layers. (**A**) A picture of the 14th century painting [*St. John the Evangelist Reproving the Philosopher Crato* by Francescuccio di Cecco Ghissi, North Carolina Museum of Art (1375)]. Inset is a magnified image showing the grey degradation on/in the vermilion pigment layer. A cross-sectional sample was taken from the indicated area. (**B**) Pump-probe image of the cross-section sample was acquired at 720 and 817 nm, 0.3 mW each, $\tau = 260$ fs. Squares in this image indicate ROIs (magenta, ROI1; red, ROI2; green, ROI3; cyan, ROI4; blue, ROI5), with their pump-probe signals shown in (C). Inset on the left side is the bright-field image of a cross section, and inset on the right side is the confocal reflectance image of the identical FOV. (**C**) Extracted pump-probe responses from the cross section at locations indicated in (B) (photo courtesy of the North Carolina Museum of Art).

pump-probe signal variations of visibly undegraded vermilion (areas of ROI2 to ROI5 in Fig. 4C), we saw no clear evidence of elemental ratio changes between Hg and S. To help elucidate the origin of the pump-probe signal as a function of crystalline phase, follow-up micro-XRD studies are in preparation.

In summary, we show that nonlinear optical absorption generated from TPA can induce a phase conversion of α- to β-HgS. The conversion is enhanced by the presence of β-HgS, likely through local sample heating due to linear absorption. Furthermore, we observed that UV exposure can produce both β-HgS and metallic Hg and that elevated temperatures accelerate this process. We also observed long-lived ESA signals during the degradation process, an effect that is under investigation. Last, we detected areas of increased concentration of β-HgS in areas of visible vermilion degradation in a 14th century painting. While Cl-assisted Hg production has been established as a degradation pathway in vermilion, our studies point to HgS phase conversion as an alternate degradation pathway in the absence of Cl. Furthermore, the detection of ESA signals in visibly undegraded vermilion layers could indicate the presence of early-stage degradation of vermilion.

MATERIALS AND METHODS

Preparation of red and black HgS

Pump-probe imaging studies

To reduce the chance for laser-induced degradation on red and black HgS, the powder was embedded in agarose gel (the gel enhances the heat diffusion), see Fig. 1. First, powder was placed on the glass slide. Agarose powder (1 g) was mixed with 10 ml of water and heated at mild temperature until the mixture turned transparent. Then, the transparent solution was applied onto the powder, and after about 30 s, the solution turned to gel. Then, the sample was covered with a coverslip.

XRD and SEM-EDS analysis

Double-sided tape was placed on a glass slide (size, 2 cm by 2 cm), then red or black HgS powder was placed on the tape.

Preparation of liquid Hg

Liquid Hg was transferred on a glass slide and then covered with a coverslip. The edge of the coverslip was sealed with glue.

Preparation of fs-laser–induced degradation of red HgS

Pump-probe imaging studies

Red HgS powder was placed between a glass slide and a coverslip and then placed in the pump-probe microscope, as shown in Fig. 2 (A to C). The imaging conditions were: pump-probe, 720 and 817 nm; 256 × 256 pixels; dwell time, 20 μs; and number of τ points, 56 (from −8 to 52 ps). Figure 2A was acquired at 0.45/0.45 mW, then one set of pump-probe images was acquired at 0.45/0.9 mW. After slight phase conversion was observed, the pump-probe power was readjusted to the original power levels (0.45/0.45 mW) to monitor the surface changes (Fig. 2B). Then, two sets of pump-probe images were acquired at 0.9/0.45 and 0.9/0.9 mW to induce more severe degradation. Figure 2C was subsequently acquired at 0.45/0.45 mW.

XRD and SEM-EDS analysis

Red HgS powder was placed between a glass slide and a coverslip; the edges were sealed with plastic tape. The glass slide was placed in the pump-probe microscope, and the surface of red HgS was scanned at a very high power to induce damage: pump-probe, 720 and 817 nm, 2.3/5 mW, τ = 0 fs; image FOV, 350 μm by 350 μm; 128 × 128 pixels; and pixel dwell time, 20 μs. Once the conversion (negative pump-probe signal) was observed, the sample was translated in the x or y direction by one FOV (350 μm). See a picture of the sample in fig. S3A.

Preparation of UV-induced degradation of red HgS

UV light delivered through a fiber bundle to red HgS powders on a microscope slide

Red HgS powder (50 mg) was placed on a glass slide, and the surface was flattened (Fig. 3, A and B). UV light from an Hg lamp was exposed on the powder (UV exposure intensity, 4.06×10^4 mW/cm^2). After exposure, the sample was transferred to the microscope.

UV light delivered through the optical system in the microscope

Red HgS powder (50 mg) was placed on the glass slide, and the surface was flattened (Fig. 3C). UV light was exposed onto the surface (UV exposure intensity, 1.14×10^4 mW/cm^2), and pump-probe signal changes were recorded over time.

UV light delivered through a fiber bundle to red HgS powders in a glass vial

Red HgS powder (0.5 g) was placed in a 20-ml glass vial, and the vial was covered with white paper (Fig. 3, D to F, and fig. S8). UV light from a Hg lamp was used to expose the powder for 5 min (UV exposure intensity, 6.55×10^4 mW/cm^2).

Apparatus

XRD analysis

X-ray diffractograms were acquired with a PANalytical X'Pert^3 Pro Materials Research Diffractometer high-resolution XRD system with a 1/2° slit, a step size of 0.05°, an acquisition time per step of 1 s, and Cu-Ka radiation (generator voltage, 45 kV; tube current, 40 mA).

Scanning electron microscopy with energy dispersive x-ray spectroscopy

A FEI XL30 ESEM with Bruker XFlash 4010 EDS detector was used for the characterization (primary voltage, 20 keV; working distance, 15 mm).

Pump-probe microscopy

A mode-locked Ti:Sapphire laser (Chameleon, Coherent) and an optical parametrical oscillator (Mira-OPO, Coherent) generate two ultrashort laser pulse trains of different wavelengths (fig. S1). An acousto-optic modulator modulates the amplitude of one of the two beams at 2 MHz (this beam is termed the pump beam), the other remains unmodulated (probe beam). The interpulse delay (τ) can be changed by adjusting the relative path length. The two pulse trains were spatially combined and focused onto the sample with a 20× 0.7 numerical aperture dry objective lens. At the focus, nonlinear interactions cause a modulation transfer from the pump pulse to the probe train. The transferred modulation in the backscattered probe beam was measured with a lock-in amplifier. A data acquisition computer records these pump-probe signals as a function of lateral position (x, y) and the interpulse time delay (τ).

UV light source

An X-Cite 120 (Hg Arc lamp, 120 W) fluorescence illuminator was used as UV source.

Damage threshold fluence

The damage threshold for illumination in Fig. 2 was experimentally determined to be 0.45 mW for the pump and probe beam when repeatedly scanning over the sample (the pulse delays were scanned). For the probe beam, an average power of 0.45 mW corresponds to a

pulse energy of 5.6 pJ. Focusing the 150-fs pulse to a 400-nm radius beam in the microscope results in a temporal peak intensity of 7.5 GW/cm^2 and an average intensity of 90 kW/cm^2. For a stationary beam, this would correspond to a fluence of 1.1 mJ/cm^2, but because of the beam, scanning the average fluence is 17 nJ/cm^2. For the modulated pump beam, the average fluence is the same, while the peak fluence roughly doubled.

SUPPLEMENTARY MATERIALS

Supplementary material for this article is available at http://advances.sciencemag.org/cgi/content/full/5/6/eaaw3136/DC1

Fig. S1. Pump-probe experimental setup and imaging contrasts.
Fig. S2. Origin of pump-probe signals and power scaling of red HgS powder.
Fig. S3. Characterizations of fs-laser–induced degradation products.
Fig. S4. SEM-EDS analysis results.
Fig. S5. Signal changes from TPA to ESA to GSD during laser-induced phase conversion and longevity of the ESA signals.
Fig. S6. Degradation studies on red HgS using different pulse durations.
Fig. S7. Increase in ESA signals during degradation under UV illumination.
Fig. S8. Characterization of UV-induced degradation products.
Fig. S9. Pump-probe images and delay traces of UV-degraded red HgS.
Fig. S10. SEM-EDS analysis on a cross-section sample.

REFERENCES AND NOTES

1. P. Ballirano, M. Botticelli, A. Maras, Thermal behaviour of cinnabar, α-HgS, and the kinetics of the β-HgS (metacinnabar) → α-HgS conversion at room temperature. *Eur. J. Mineral.* **25**, 957–965 (2013).
2. S. Adachi, in *Handbook on Physical Properties of Semiconductors* (Springer US, 2004), vol. 3, pp. 403–418.
3. M. A. Nusimovici, A. Meskaoui, Raman scattering by α-HgS (cinnabar). *Phys. Stat. Sol. B* **58**, 121–125 (1973).
4. B. Pal, S. Ikeda, B. Ohtani, Photoinduced chemical reactions on natural single crystals and synthesized crystallites of mercury (II) sulfide in aqueous solution containing naturally occurring amino acids. *Inorg. Chem.* **42**, 1518–1524 (2003).
5. E. Doni, L. Resca, S. Rodriguez, W. M. Becker, Electronic energy levels of cinnabar (α-HgS). *Phys. Rev. B* **20**, 1663–1668 (1979).
6. M. Cardona, R. K. Kremer, R. Lauck, G. Siegle, A. Muñoz, A. H. Romero, Electronic, vibrational, and thermodynamic properties of metacinnabar β-HgS, HgSe, and HgTe. *Phys. Rev. B* **80**, 195204 (2009).
7. M. K. Neiman, M. Balonis, I. Kakoulli, Cinnabar alteration in archaeological wall paintings: An experimental and theoretical approach. *Appl. Phys. A* **121**, 915–938 (2015).
8. R. Nöller, Cinnabar reviewed: Characterization of the red pigment and its reactions. *Stud. Conserv.* **60**, 79–87 (2015).
9. N. Melniciuc-Puică, E. Ardelean, N. Vornicu, Red pigments used for writing and illuminating manuscripts. *An. Stiint. Univ. "Al. I. Cuza" Iasi* **2013**, 75–87 (2013).
10. M. Spring, R. Grout, The blackening of vermilion: An analytical study of the process in paintings. *National Gallery Technical Bulletin* **23**, 50–61 (2002).
11. W. Anaf, K. Janssens, K. De Wael, Formation of metallic mercury during photodegradation/photodarkening of α-HgS: Electrochemical evidence. *Angew. Chem.* **125**, 12800–12803 (2013).
12. C. Miliani, L. Monico, M. J. Melo, S. Fantacci, E. M. Angelin, A. Romani, K. Janssens, Photochemistry of artists' dyes and pigments: Towards better understanding and prevention of colour change in works of art. *Angew. Chem. Int. Ed.* **57**, 7324–7334 (2018).
13. R. S. Davidson, C. J. Willsher, The light-induced blackening of red mercury (II) sulphide. *J. Chem. Soc. Dalton Trans.* **1981**, 833–835 (1981).
14. H. Béarat, A. Chizmeshya, R. Sharma, A. Barbet, M. Fuchs, Mechanistic and computational study of cinnabar phase transformation: Applications and implications to the preservation of this pigment in historical paintings, in the *Third International Conference on Science and Technology in Archaeology and Conservation*, Jordan, 7 to 11 December 2004, pp. 53–70.
15. P. Vandenabeele, K. Lambert, S. Matthys, W. Schudel, A. Bergmans, L. Moens, In situ analysis of mediaeval wall paintings: A challenge for mobile Raman spectroscopy. *Anal. Bioanal. Chem.* **383**, 707–712 (2005).
16. M. Oujja, M. Sanz, E. Rebollar, J. F. Marco, C. Domingo, P. Pouli, S. Kogou, C. Fotakis, M. Castillejo, Wavelength and pulse duration effects on laser induced changes on raw pigments used in paintings. *Spectrochim. Acta A Mol. Biomol. Spectrosc.* **102**, 7–14 (2013).
17. V. Zafiropulos, C. Balas, A. Manousaki, Y. Marakis, P. Maravelaki-Kalaitzaki, K. Melesanaki, P. Pouli, T. Stratoudaki, S. Klein, J. Hildenhagen, K. Dickmann, B. S. Luk'Yanchuk, C. Mujat, A. Dogariu, Yellowing effect and discoloration of pigments: Experimental and theoretical studies. *J. Cult. Herit.* **4**, 249–256 (2003).
18. C. Miguel, J. V. Pinto, M. Clarke, M. J. Melo, The alchemy of red mercury sulphide: The production of vermilion for medieval art. *Dyes Pigm.* **102**, 210–217 (2014).
19. F. W. Dickson, G. Tunell, The stability relations of cinnabar and metacinnabar. *Am. Mineral.* **44**, 471–487 (1959).
20. J. K. McCormack, The darkening of cinnabar in sunlight. *Miner. Deposita* **35**, 796–798 (2000).
21. M. Radepont, Y. Coquinot, K. Janssens, J.-J. Ezrati, W. de Nolf, M. Cotte, Thermodynamic and experimental study of the degradation of the red pigment mercury sulfide. *J. Anal. At. Spectrom* **30**, 599–612 (2015).
22. W. Anaf, S. Trashin, O. Schalm, D. van Dorp, K. Janssens, K. de Wael, Electrochemical photodegradation study of semiconductor pigments: Influence of environmental parameters. *Anal. Chem.* **86**, 9742–9748 (2014).
23. K. Keune, J. J. Boon, Analytical imaging studies clarifying the process of the darkening of vermilion in paintings. *Anal. Chem.* **77**, 4742–4750 (2005).
24. F. Da Pieve, C. Hogan, D. Lamoen, J. Verbeeck, F. Vanmeert, M. Radepont, M. Cotte, K. Janssens, X. Gonze, G. Van Tendeloo, Casting light on the darkening of colors in historical paintings. *Phys. Rev. Lett.* **111**, 208302 (2013).
25. M. Cotte, J. Susini, V. A. Solé, Y. Taniguchi, J. Chillida, E. Checroun, P. Walter, Applications of synchrotron-based micro-imaging techniques to the chemical analysis of ancient paintings. *J. Anal. At. Spectrom* **23**, 820–828 (2008).
26. J. M. Charnock, L. N. Moyes, R. A. D. Pattrick, J. F. W. Mosselmans, D. J. Vaughan, F. R. Livens, The structural evolution of mercury sulfide precipitate: An XAS and XRD study. *Am. Mineral.* **88**, 1197–1203 (2004).
27. M. O. Barnett, L. A. Harris, R. R. Turner, R. J. Stevenson, T. J. Henson, R. C. Melton, D. P. Hoffman, Formation of mercuric sulfide in soil. *Environ. Sci. Technol.* **31**, 3037–3043 (1997).
28. P. Pouli, D. C. Emmony, C. E. Madden, I. Sutherland, Studies towards a thorough understanding of the laser-induced discoloration mechanisms of medieval pigments. *J. Cult. Herit.* **4**, 271–275 (2003).
29. K. Janssens, G. Van der Snickt, F. Vanmeert, S. Legrand, G. Nuyts, M. Alfeld, L. Monico, W. Anaf, W. De Nolf, M. Vermeulen, J. Verbeeck, K. De Wael, Non-invasive and non-destructive examination of artistic pigments, paints, and paintings by means of X-ray methods. *Top. Curr. Chem.* **374**, 81 (2016).
30. M. C. Fischer, J. W. Wilson, F. E. Robles, W. S. Warren, Invited review article: Pump-probe microscopy. *Rev. Sci. Instrum.* **87**, 031101 (2016).
31. J. Yu, W. S. Warren, M. C. Fischer, Spectroscopic differentiation and microscopic imaging of red organic pigments using optical pump–probe contrast. *Anal. Chem.* **90**, 12686–12691 (2018).
32. T. E. Villafana, W. P. Brown, J. K. Delaney, M. Palmer, W. S. Warren, M. C. Fischer, Femtosecond pump-probe microscopy generates virtual cross-sections in historic artwork. *Proc. Natl. Acad. Sci. U.S.A.* **111**, 1708–1713 (2014).
33. T. E. Villafana, J. K. Delaney, W. S. Warren, M. C. Fischer, High-resolution, three-dimensional imaging of pigments and support in paper and textiles. *J. Cult. Herit.* **20**, 583–588 (2016).

Acknowledgments: We would like to thank W. Brown from the North Carolina Museum of Art for the advice and procurement of cross-section samples. We also thank J. Delaney for valuable assistance and discussions. **Funding:** This material is based on work supported by the National Science Foundation Division of Chemistry under award no. CHE-1610975 (to M.C.F.). **Author contributions:** J.Y. prepared all samples, performed all experiments, and analyzed the data. W.S.W. and M.C.F. supervised the project and participated in data interpretation. **Competing interests:** The authors declare that they have no competing interests. **Data and materials availability:** All data needed to evaluate the conclusions in the paper are present in the paper and/or the Supplementary Materials. Additional data related to this paper may be requested from the authors. Correspondence and requests for materials should be addressed to M.C.F. (martin.fischer@duke.edu).

Submitted 23 January 2019
Accepted 14 May 2019
Published 21 June 2019
10.1126/sciadv.aaw3136

Citation: J. Yu, W. S. Warren, M. C. Fischer, Visualization of vermilion degradation using pump-probe microscopy. *Sci. Adv.* **5**, eaaw3136 (2019).